Multifunctional Ionic Hydrogel Based Transdermal Delivery of 5-Fluorouracil for the Breast Cancer Treatment

Raviraj Pansuriya[a], Tapas Patel[a], Sugam Kumar[b], Vinod K Aswal[b], Naina Raje[c], Clare Hoskins[d], Suresh Kumar Kailasa[a], Naved I. Malek[a]*

[a]Ionic Liquids Research Laboratory, Department of Chemistry, Sardar Vallabhbhai National Institute of Technology, Surat-395007, Gujarat, India

[b]Solid State Physics Division, Bhabha Atomic Research Centre, Trombay, Mumbai-400085, India

cAnalytical Chemistry Division, Bhabha Atomic Research Centre, Trombay, Mumbai-400085, India

[d] Technology and Innovation Centre, Department of Pure and Applied Chemistry, University of Strathclyde, Glasgow G1 1RD, UK

Corresponding Author e-mail: navedmalek@chem.svnit.ac.in

Abstract

Transdermal drug delivery systems (TDDS) are a promising and innovative approach for breast cancer treatment, offering advantages such as non-invasiveness, potential for localized and prolonged drug delivery while minimizing systemic side effects through avoiding first-pass metabolism. Utilizing the distinctive characteristics of hydrogels, such as their biocompatibility, versatility, and higher drug loading capabilities, in the present work we prepared ionic hydrogels through synergistic interaction between ionic liquids (ILs), Choline Alanine ([Cho][Ala]) and Choline Proline ([Cho][Pro]) with oleic acid (OA). ILs used in the study are biocompatible and enhance the solubility of 5-Fluorouracil (5-FU), whereas OA is a known chemical penetration enhancer. Concentration dependent (OA) change in morphological aggregates, i.e. from cylindrical micelles to worm-like micelles to hydrogels was formed with both ILs and were characterized by SANS measurement, whereas the interactions involved were confirmed by FTIR spectroscopy. The hydrogels owes excellent mechanical properties, studied by rheology and its morphology through FE-SEM analysis. The *in vitro* skin permeation study revealed that both hydrogels penetrated 255 times ([Cho][Ala]) and 250 times ([Cho][Pro]) more as compared to PBS after 48 h. Those ionic hydrogels exhibited the capability to change the lipid and keratin

This is a peer-reviewed, accepted author manuscript of the following article: Pansuriya, R., Patel, T., Kumar, S., Aswal, V. K., Raje, N., Hoskins, C., Kumar Kailasa, S., & Malek, N. I. (in press). Multifunctional ionic hydrogel based transdermal delivery of 5-fluorouracil for the breast cancer treatment. ACS Applied Bio Materials.

arrangements within the skin layer, thereby enhancing the transdermal permeation of the 5-FU. Both ionic hydrogels exhibit excellent biocompatibility with normal cell lines (L-132 cells), as well as cancerous cell lines (MCF-7 cells), demonstrating over 92 % cell viability after 48 h in both cell lines. *In vitro*, cytotoxicity of the 5-FU loaded hydrogels was evaluated on MCF-7 and HeLa cell lines. These results indicate that the investigated biocompatible and non-toxic ionic hydrogels enable the transdermal delivery of hydrophilic drugs, making them a viable option for effectively treating breast cancer.

Keywords: Transdermal Drug Delivery Systems; Hydrogel; Ionic Liquid; Oleic acid; 5-Fluorouracil; Skin Penetration Enhancer; Breast Cancer.

Introduction

Breast cancer is a widespread issue in various regions of the world.[1,2] The standard approaches including chemotherapy or radiation therapy are available to treat breast cancer. However, in certain cases where surgery is not possible or recommended, chemotherapy could be a more suitable option; however, some side effects are observed after treatment.[3] Transdermal drug delivery systems (TDDSs) offer several key benefits in comparison to traditional treatments as well as injectable and oral methods.[4] These advantages include circumventing the ability to bypass enzymatic degradation, the initial metabolic impact from the liver and diaphragm, ensuring extended therapeutic presence, and enhancing patient adherence to treatment.[5] Still, TDDSs have certain complications in drug delivery, specifically when it comes to hydrophilic and high-molecular-weight substances such as proteins and peptides.[6] Predominantly due to the formidable barrier imposed by the skin's robust hydrophobic outer layer, known as the stratum corneum (SC). To overcome this drawback, various approaches have been reported, which encompass the implementation of chemical agents that enhance permeation and physical methods such as microneedles or electroporation ablation to diminish the barrier.[7] The physical methods require instruments and injure the skin while penetrating, making the chemical enhancers efficient for transdermal delivery.[8] Numerous chemical permeation enhancers (CPEs) such as sulfoxide, menthol ester derivatives, and ethanol are traditionally used for improving drug

permeation, but they suffer of skin toxicity and irritation behaviour.[9,10] To address these, fatty acids based CPEs are studied in recent times because of its low toxicity and negligible skin irritation.[11,12] Apart from these, solubility of the drugs in pharmaceutically approved solvent also limit their application as the TDD.[5] To resolve these limitations, ionic liquid (IL) based drug delivery systems have been investigated thoroughly. Basically, ILs are liquid at room temperature and/or melt below 100 °C because cations and anions are arranged in an asymmetric manner and possess several unique physico-chemical properties.[13]

In the prior investigations, numerous efforts were made to develop IL based TDDSs in various forms, including micelles, lipid bilayers and emulsions-based systems to name a few.[14–16] However, these systems face challenges related to biocompatibility with normal cells. Previously hydrophobic ILs were prepared from imidazolium as cation with different types of anions such as hexafluorophosphate and tetrafluoroborate as an excellent skin penetration enhancer. However, these ILs are lacking of biocompatibility and biodegradability.[17,18] To circumvent these limitations, biocompatible fatty acid based ILs are recently used as the TDDs in a form of microemulsion, that enhances skin permeation as well as solubility of anti-inflammatory drug.[19] In TDDSs, the contact time with the skin plays a crucial role in facilitating drug penetration, which increases the requirement of adhesiveness, along with mechanical stability and self-healing capacity.[20,21] Designing hydrogel with outstanding biocompatibility, remarkable swelling capacity, robust mechanical characteristics, adhesiveness, significant drug encapsulation capacity, and the ability to respond to external stimuli could circumvent all these shortcomings and could be the best choice as the new age TDDs.[22,23] Recently, the IL based polymeric hydrogel was used as a system for TDDs in wound healing.[24] However, the preparation of these kind of systems is quite lengthy using various reagents including crosslinkers. To overcome these challenges, we need a system, which is an easy to prepare, biocompatible, self-healable, and adhesive, having high mechanical properties as well as enhanced solubility of drugs.

In our efforts to prepare smart TDDs, in the present investigation we have designed biocompatible, stimuli-responsive, adhesive, and self-healable ionic hydrogels as the new age TDDSs. ILs used in the study have choline as the cation and alanine and proline as the anions and are denoted as [Cho][Ala] and [Cho][Pro] respectively. Both ILs are synthesized from natural origins and are biocompatible.[25] Although these ILs increases the solubility of the chemotherapeutic drug 5-Fluorouracil (5-FU), they could not efficiently penetrate through the skin with the drug because of their hydrophilic nature and inability to form hydrogel itself. To overcome this limitation, we introduced oleic acid (OA) as a skin penetration enhancer. Additionally, OA plays a multifaceted role in biocompatibility, self-healing and adhesive properties of the hydrogel, as it has ability to form various nano-aggregates including ionic hydrogel through synergistic interaction with ILs.[26] These aggregates within the hydrogel can contribute to the self-healing properties of the hydrogel by promoting molecular rearrangement and reformation of the gel structure upon mechanical damage. Further, these aggregates also enhance adhesiveness by interactions with the substrate surface including hydrogen bonding or hydrophobic interactions. Furthermore, OA exhibit biocompatibility and do not pose harmful effect on healthy tissues. We have characterized the hydrogels and their mechanical properties using various state of the art analytical techniques including SANS, FE-SEM, FTIR, and rheological analysis in detail. To assess the skin permeation of 5-FU utilizing these ionic hydrogels and their impact on skin barrier function, we conducted experiments on goat skin through the Franzen diffusion cell. Additionally, we evaluated the *in vitro* biocompatibility of ionic hydrogels using normal cell lines (M132 cells) as well as cancerous cell lines (MCF-7 and HeLa cells). Further, the effectiveness and IC_{50} of 5-FU loaded ionic hydrogels were assessed through performing *in vitro* cytotoxicity study on MCF-7 and HeLa cell lines.

Methods and Materials

Materials

Alanine, proline, and oleic acid (OA) were purchased from SRL (Sisco Research Laboratory, India). 5-Fluorouracil, 47–50% choline hydroxide, and PBS 7.4 capsules were received from TCI (Tokyo Chemical Industry, Japan). During all experiments, we used double-distilled deionized water. All chemicals are of reagent grade and used as received.

Synthesis of Ionic Liquids

Amino acid and choline-based ILs were synthesised by previously reported methods with slight modifications.[25,27] In brief, the amino acid (1.01 eq) was added to the choline hydroxide solution (1.0 eq) in the round bottom flask. This mixture was stirred at 800 rpm in dark conditions and maintained a reaction temperature between 0-5 °C. After the reaction was completed, the water was removed by a rotary evaporator. The unreacted amino acid was precipitated out by the addition of acetonitrile and separated by filtration. Furthermore, acetonitrile was removed by a rotary evaporator, and a slightly yellowish liquid product was obtained. Both ILs ([Cho][Ala], [Cho][Pro]) were characterised by ^{1}H-NMR spectroscopy for any probable impurities (**Figure S1**).

Preparation of Ionic Hydrogels

The ionic hydrogels were prepared through interacting ILs with OA (**Scheme 1**). Briefly, 0.80 M solution of both ILs were kept at room temperature(25°C), followed by the dropwise addition of OA keeping in vortex in order to get homogeneity. Once the OA concentration reached 0.70 M and 0.75 M, the [Cho][Ala] and [Cho][Pro] based ionic hydrogel were formed, respectively. The data based on the visual observation of systems at different concentrations of all components are shown in **Table 1**. It is important to mention here that once the concentration of OA reaches 0.80 M and higher, stiff hydrogels were formed. At this concentration, solubility of 5-FU decreases. Further, increasing the concentration of ILs to 0.95 mM, we needed lesser amount of OA but the hydrogel show limited skin permeation.

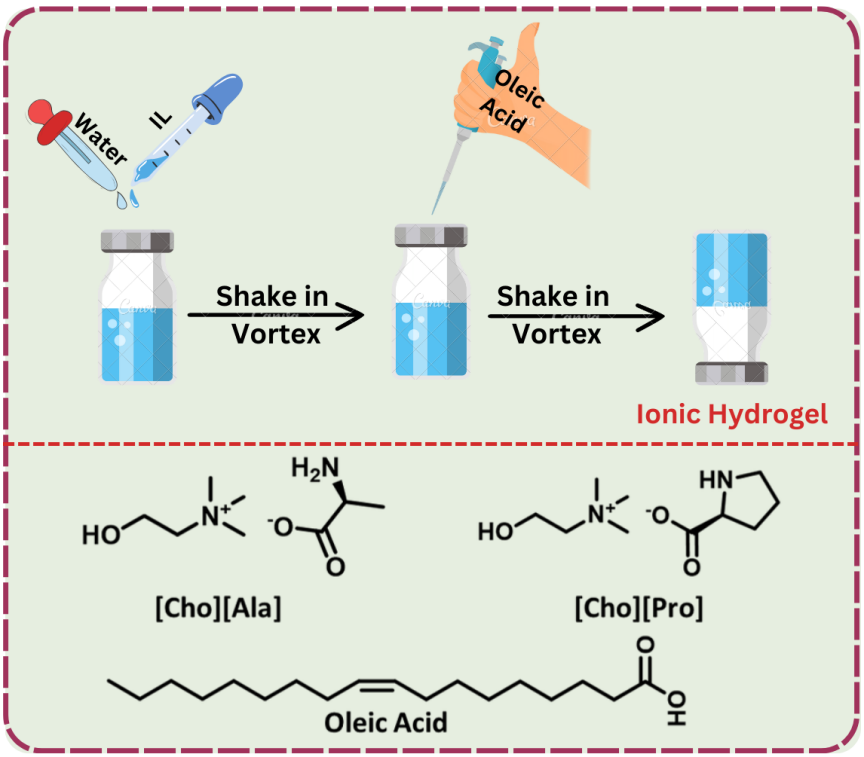

Scheme 1: Preparation process of the ionic hydrogels.

Table 1: Concentration of ILs and oleic acid in ionic hydrogels, pH of the systems.

[Cho][Ala] (M)	[OA] (M)	pH	Phase	[Cho][Pro] (M)	[OA] (M)	pH
0.80	0.0	12.5	Solution	0.80	0.0	13.0
0.80	0.21	11.1	Solution	0.80	0.15	10.1
0.80	0.42	10.0	Viscous Solution	0.80	0.33	9.7
0.80	0.50	8.2	Loose Gel	0.80	0.45	8.5
0.80	0.66	7.0	Gel	0.80	0.60	7.0
0.80	0.80	7.0	Gel	0.80	0.80	7.0

FT-IR

Interactions present within ionic hydrogels were investigated by FTIR spectroscopy. For this purpose, we used a Jasco FTIR instrument with 400 to 4000 cm^{-1} range and 45 scans. We have recorded FTIR spectra of both hydrogels, [Cho][Ala], [Cho][Pro], as well as oleic acid.

SANS

SANS analysis of all formulations was conducted in SANS-1 diffractometer at Guide Tube laboratory, Dhruva reactor, BARC, Mumbai, India. We performed SANS experiments of both hydrogels with a fixed concentration of IL (For both, the concentration of ILs is 0.80 M) and various concentrations of OA (0 to 0.66 M). All samples are prepared in D_2O for SANS analysis and experimental data are analysed in SasView software using different fitting models including cylindrical micelles, flaxible cylinder model and broad peak model.

FE-SEM

The morphology of both ionic hydrogels was analysed by FE-SEM (Hitachi S-4800 N), operated at 5000 V. To increase conductivity and imaging quality, the hydrogel samples were coated with a small layer of gold particles. Furthermore, elemental analysis of the hydrogels is done by energy-dispersive X-ray spectroscopy (EDS).

Mechanical Properties

Mechanical properties of [Cho][Ala] and [Cho][Pro] based ionic hydrogels were performed on Anton Paar Physical MCR-301 rheometer. We used parallel plates with a diameter of 25 mm with 1.0 mm of gap. The viscosity of hydrogels was measured against the shear rate from 0 to 100 (1/s). The strain sweep test was performed at 0 to 200 % strain against modulus (G' and G") with constant angular frequency (1 rad/s). The frequency sweep test was measured within the range of 0 to 100 rad/s of angular frequency against modulus (G' and G") with a constant strain value of 1%.

TGA and DSC

SDT Q600 V20.9 Build 20 TGA instrument was used to determine the thermal stability and decomposition behavior of both ionic hydrogels. The samples with 7.0 mg were taken in an aluminum pan and heated from 20 to 500 °C with a 5 °C/min heating rate under 100 mL/min nitrogen flow. Additionally, the Mettler-Toledo DSC (Model DSC3/700/761) apparatus was used to observe the temperature effect on both hydrogels. For this purpose, we used an aluminum pan and samples were

heated from 25 to 150 °C with a 5 °C/min heating rate under a nitrogen atmosphere.

Self-healing Property of Ionic Hydrogels

The self-healing behaviour of hydrogels was investigated by a conventional method. For better visual observation, two different colour dyes loaded hydrogel were used at the minimum concentrations of dyes. Both dyes loaded hydrogels were shaped using circular moulds followed by cutting them into half pieces and placing them together again with alternative dyes. Further, the self-healed hydrogels were tested manually by stretching them. For more detailed elaboration, the self-healing behaviour of both hydrogels was investigated by a relaxation test. That includes four cycles of measuring the modulus (G' and G") against the different strain values (lower strain = 5%, higher strain = 30%) at a constant angular frequency of 1 rad/s.

Adhesive Properties of Ionic Hydrogels

The lap-shear test was performed to explore the adhesive properties of ionic hydrogels. In brief, hydrogel samples were placed between different substrates (skin, rubber, steel) with a contact area of 8 × 20 mm^2. By studying the displacement distance caused by adhesive stress, the adhesive strength of ionic hydrogels was measured.

Drug-Loading

The physical entrapment method was used for drug loading in ionic hydrogels. In this method, we dissolved 5-FU at its saturated concentration in an aqueous solution of ILs (0.8 M) followed by adding an OA to form hydrogels. The amount of 5-FU in hydrogels was measured through UV spectroscopy, and the drug loading capacity of the hydrogel was measured by the following **equation 1**:

$$Drug\ Loading = \frac{Ammount\ of\ Drug\ Loaded\ in\ hydrogel}{Weight\ of\ Hydrogel} \times 100 \qquad (1)$$

Effects of ILs, Ionic Hydrogels on the SC Layer of Skin

We used goat skin to determine the mechanism of skin permeation. We performed this process by the previously reported method, The frozen goat skin samples were defrosted at room temperature, and then any remaining blood was rinsed off with phosphate-buffered saline (PBS). Warm the skin for two minutes at 60 °C to remove moisture. To separate the epidermis from the thick skin, the skin was scratched. This separated epidermis was immersed in a trypsin and EDTA solution for 24 hours at room temperature in order to extract SC layer. The isolated SC was washed with ethanol and dried at room temperature. This isolated SC was placed in hydrogels made of [Cho][Ala], [Cho][Pro] as well as in PBS (control) for 12 hours. Hydrogels and PBS containing SC layer washed with ethanol and dried. That SC was examined using an FTIR spectroscopic technique to know the skin permeation mechanism.

In Vitro Skin Permeation Study

A Franz diffusion cell was used to investigate the *in vitro* skin permeation of 5-FU from ionic hydrogels. Goat skin was placed between the donor chamber and the receptor chamber; the drug-loaded hydrogel was placed in the donor chamber; and 7.4 pH PBS was filled in the receptor chamber. The temperature of the receptor chamber was maintained at 32 °C with a continued flow of water in the water jacket. Take a 0.5-mL sample from the receptor chamber through the sampling port at regular time intervals and add the same amount of fresh PBS to the receptor chamber. UV-Vis spectroscopy was used to measure the drug amount. The data obtained from *in vitro* skin permeation experiments are used to derive the skin permeation parameters. Transdermal flux was calculated through the slope method as shown in **equation 2** and the permeation coefficient was calculated by **equation 3**.

$$J = \frac{Slope}{A} \tag{2}$$

Where A is effective surface area of the skin

$$Kp = \left(\frac{J}{C_o}\right) \tag{3}$$

Kp is the permeability coefficient, j is transdermal flux, and C_o initial concertation of drug in the hydrogel.

In vitro Biocompatibility and Cytotoxicity of the Ionic Hydrogels

Biocompatibility of both ionic hydrogels was performed on normal cell lines (M-132 cells) and breast cancer cell lines (MCF-7 cells). During experiments, we used a 96-well plate with 1×10^5 cells per well, Dulbecco's Modified Eagle Medium (DMEM), and fetal bovine serum for cell growth. The different concentrations of ionic hydrogels (0, 0.96, 1.92, 3.54, 7.69, and 11.53 mg/mL) were placed in wells containing cells for 48 h. The cell viability was determined by the MTT assay, and the cell viability of each concentration of hydrogel was compared with the positive control (without hydrogel). The same process was followed for the cytotoxicity evolution of drug-loaded hydrogels on two different cell lines (MCF-7 and HeLa cell lines). The drug concentration was taken: 0.0, 0.96, 1.92, 3.54, and 11.53 mM in the ionic hydrogels. The IC_{50} of both hydrogels after 48 hours for MCF-7 and HeLa cell lines was obtained.

Results and discussion

The ionic hydrogels were prepared through synergistic interaction between Choline-Amino Acid Ionic Liquids (CAAILs) and OA. At fixed concentrations of CAAILs, concentration of OA was increased and the change in the solution viscosity and pH of the system was noticed (**Table 1**). At certain concentration of OA, viscosity of the solution increased followed by the conversion of an ionic hydrogel. This may be due to the increased interactions between aggregate formed by OA at higher concentrations and ILs. We used Small Angle Neutron Scattering (SANS) measurements to confirm the formation and conversion of all kinds of aggregates and their size and shapes. As shown in **Figure 1,** the SANS curve and fitting model for [Cho][Ala] and [Cho][Pro] based systems, indicates that the shape and size of all aggregates depend upon the concentration of OA. In the [Cho][Ala] based system (**Figure 1a**), no scattering was observed in the absence of OA (0.0 M), suggesting the absence of aggregates in the system. Increasing concentration of OA to 0.21 M altered the scattering curve, with lower and mid q ranges displaying higher intensity and higher q ranges showing lower intensity. Model

fitting confirmed cylindrical micelles present at 0.21 M OA. Additionally, when the concentration of OA was raised to 0.42 and 0.50, it lead to changes in the scattering curve across the higher, mid, and lower q ranges. The fitting model revealed a structure conversion from cylindrical micelles to worm-like micelle to viscous solution (**Scheme 2**). The SANS curve of this viscous solution aligns with the broad peak model (Additional information is provided in ESI file). According this model the Lorentz length signifies the mash size of the ionic hydrogel, while the peak position having relation with the d-spacing ($q^0 = {}^{2\pi}/_{d_0}$), which can be denoted by distance between aggregates within the hydrogel. Once the OA concentration reached 0.50 M, worm-like micelles were cross-linked to each other through physical cross-liking, resulting in the formation of small aggregates. Model fitting revealed a 0.08177 1/ Å peak position and 35.12 Å mese size of loose gel. Moreover, as OA concentration increased to 0.66 M, ionic hydrogel formed, and a sharp peak was generated at a higher q value in SANS curve. Fitting parameters indicated that these small aggregates were closer to one another, forming a 3-D network structure. The distance between aggregates decreases (peak position is 0.08421 1/Å), and the mesh size for the ionic hydrogel was observed by 85.502 Å. A similar mechanism is followed in [Cho][Pro] based ionic hydrogel (**Figure 1b**), but the mesh size in this gel is higher than that in [Cho][Ala] based gel because proline has a bulky structure compared to the alanine stature. Similar broad peak model in SANS analysis was applied for the effect of temperature on the aggregation of proteins by Joseph et al[25] where the author noted that when the temperature was decreased from 20 to 0 °C, no peak was observed in the SANS curve. But once the temperature was decreased from 0 to -80 °C, and the high q peak generated indicating that at this temperature, smaller aggregates came close to each other and form a solid-like structure.[28] Likewise, concentration-dependent structure conversion from micelles to vesicles to lamellar gel of surface-active ionic liquid is explored by Kuddushi and co-workers.[29] All parameters of the fitting models are given in **Table 2** including the concentration of the ILs and OA in system. The ionic hydrogel formation and structural transformations were observed as a result of OA ability to form various types of aggregates with changes in pH values and concentrations.[26,30] Suga et al. studied

various aggregated structures of OA such as spherical micelles, cylindrical micelles, vesicles, and cubosomes merely changing the pH of the solution from 10.6 to 7.5.[26] When OA is introduced to an alkaline [Cho][Ala] aqueous solution, the pH of the system decreases (**Table 1**), which causes the system to undergo structural transformation. Additionally, those results were obtained due to non-covalent interactions present between IL and oleic acid. That non-covalent interactions were proved by FTIR spectroscopy (*vide infra).*

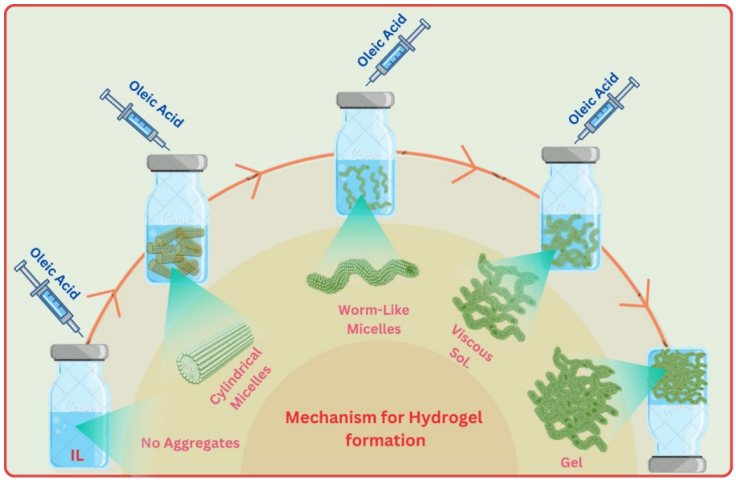

Scheme 2: A schematic representation of microstructural aggregates of system as a function of OA concentration leading to the formation of an ionic hydrogel.

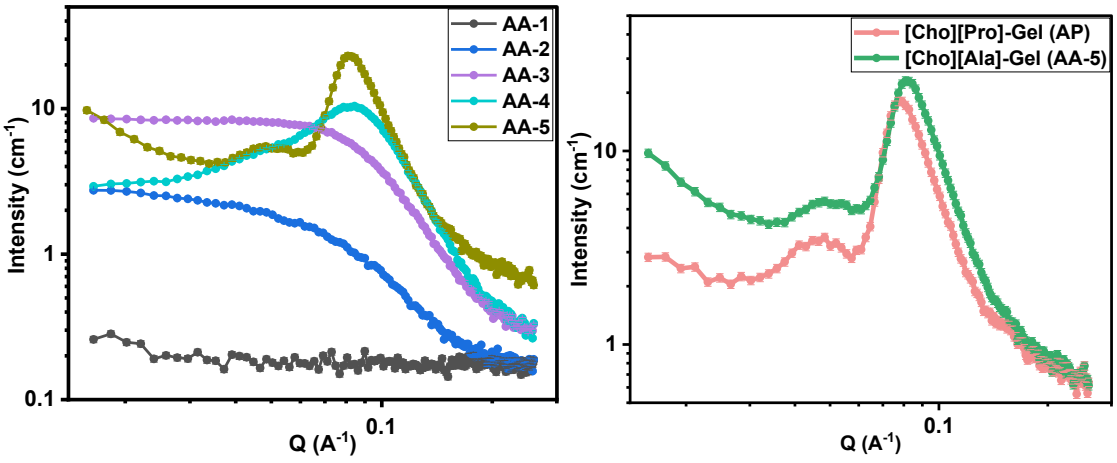

(a) (b)

Figure 1: SANS analysis of concentration dependent structural transition of **(a)** [Cho][Ala] based system, (●) is cylindrical micelles at oleic acid

(0.21 M), (●) is worm-like micelles at oleic acid (0.42 M), (●) Loose Gel at oleic acid (0.50 M) and (●) is ionic hydrogel at oleic acid (0.66 M); **(b)** (●) is [Cho][Pro] and (●) is [Cho][Ala] based ionic hydrogel.

Table 2: Parameters of various fitted model for SANS analysis.

Code	[Cho][Ala] (M)	[OA] (M)	Model	Parameters		
AA-1	0.80	0.0	No scattering	-		
AA-2	0.80	0.21	Cylindrical	**Length (Å)**	**Radius (Å)**	
				62.039	18.106	
AA-3	0.80	0.42	Worm-like	**Length (Å)**	**Kuhn Length (Å)**	**Radius (Å)**
				33.021	72.282	18.011
AA-4	0.80	0.50	Broad Peak	**Mesh size (Å)**	**Peak Position (1/ Å)**	
				35.12	0.08177	
AA-5	0.80	0.66	Broad Peak	85.502	0.08421	
AP	[Cho][Pro] 0.80	0.60	Broad Peak	93.00	0.08122	

To investigate the non-covalent molecular interactions responsible for the formation of the ionic hydrogel, we performed FTIR spectra of ionic hydrogel and compared them with neat ILs and OA. As shown in **Figure S2 a**, the characteristic peak of [Cho][Ala] was found at 3356.14 cm^{-1}, 3255.42 cm^{-1}, and 1558.48 cm^{-1} for -NH_2, OH, and COO^- stretching respectively. The hydrogen bonding and electrostatic interactions are present between the NH_2, OH, and COO^- functional groups of IL and the C=O functional group of OA. The frequency attributed to NH_2 was shifted from 3356.14 cm^{-1} to 3386.29 cm^{-1}, the frequency attributed to OH was shifted from 3255.42 cm^{-1} to 3241.02 cm^{-1} and the frequency attributed to COO^-

from 1558.1 cm^{-1} to 1548.76 cm^{-1} in the ionic hydrogel. In OA, the frequency of the C=O group was shifted from 1708 cm^{-1} to 1775 cm^{-1} in the ionic hydrogel.[31] Those results suggest that hydrogen bonding and electrostatic interaction were dominantly present between IL and OA. Similar kinds of results are observed in [Cho][Pro]-based ionic hydrogels, as shown in **Figure S2 b**.

We turned to FE-SEM to investigate the morphology of the studied hydrogels to have a better visual understanding of their internal composition and structure. The FE-SEM images (**Figure 2**) illustrate that hydrogels exhibit elongated, intertwined fibers consisting of closely packed tubules.[29] Those physically cross-linked tubules come together to form a 3D structure. The reason behind this ionic hydrogel formation is the interconversion of cylindrical micelles to worm-like micelles, which are characterised by SANS analysis (*vide supra*). Those wormlike micelles cross-linked through interdigitation resulting the formation of hydrogels. Unlike the morphology of the [Cho][Ala] based hydrogel (**Figure 2a**), the hydrogel made up of [Cho][Pro] exhibits a symmetrical arrangement of fibers, that arrangement provides an overall uniform structure (**Figure 2b**). This is due to the presence of a cyclic ring in the proline structure, which participates in interaction in a distinct way. Whereas lacking a ring in the structure of alanine is the reason for asymmetry in the morphology of [Cho][Ala] based hydrogel.[32] Similar fibrous morphology was observed in amino acid-based metallo hydrogel and also for the IL based hydrogel.[33,34]

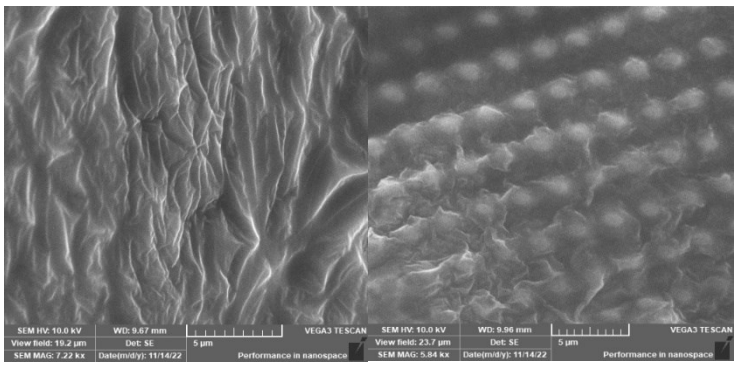

(a) (b)

Figure 2: FE-SEM analysis of ionic hydrogels (a) [Cho][Ala] based ionic hydrogel and (b) [Cho][Pro] based ionic hydrogel.

Furthermore, an EDX analyzer was used to assess the elemental composition and distribution of each element within the hydrogel.[35] The EDX spectra and SEM image of [Cho][Ala] (**Figure S3 a**) indicate that 76% C, 4% N, and 20% O are present in hydrogel, and each element was equally distributed within the hydrogel. Similarly, C, O, and N are present in [Cho][Pro]-based hydrogel with having elemental composition of 78%, 19%, and 3%, respectively. **Figure S3 b** suggests that the all elements are spread homogenously within the ionic hydrogel. For the chitosan/PVA based hydrogel similar elemental distribution of compounds was observed.[36]

Applicability of hydrogel can be predicted through knowing the mechanical stability of the hydrogel. To investigate the mechanical properties of the studied ionic hydrogels we used rheological analysis. The flowing behaviour of ionic hydrogels were investigated by measuring viscosity as function of shear rate. As shown in **Figure 3 a, d** viscosity rheo-graphs of [Cho][Ala] and [Cho][Pro] based hydrogels suggest that viscosity decreases with an increase in shear rate from 1 to 100 1/sec. This phenomenon is denoted by 'steady shear flow'.[37] These data indicate that hydrogels have a flowing behaviour, which is necessary for TDDSs. Further, the angular frequency sweep test was applied to find the mechanical stability of hydrogel as a function of modulus (G' and G''). As illustrated in **Figures 3 b and e**, the value of storage modulus (G') is higher than that of loss modulus (G''), over the 0 to 100 rad/s frequency range for both ionic hydrogels indicating the robust mechanical property at this angular frequency range. The strain sweep test was performed to identify the viscoelastic behaviour of ionic hydrogels. As depicted in **Figure 3 c and f**, cross over point (γ_c) was observed at 9.5% and 9.2% strain value for [Cho][Ala] and [Cho][Pro] based hydrogel, respectively. The region, where G' is greater than G'' (below γ_c), called an elastic region or linear region. In this region hydrogel behave like as semi-solid material. Whereas, above γ_c, G' is less than G'', which indicates that hydrogel was deformed and behaves like viscous solution. This strain sweep data indicates that hydrogels have viscoelastic behaviour. For the amino acids-based hydrogel, Jaint and coworkers have observed cross over point in strain sweep test at 5 % strain, suggesting the

higher stability in our hydrogel due to the interactions between an amino acid based IL and OA.[38]

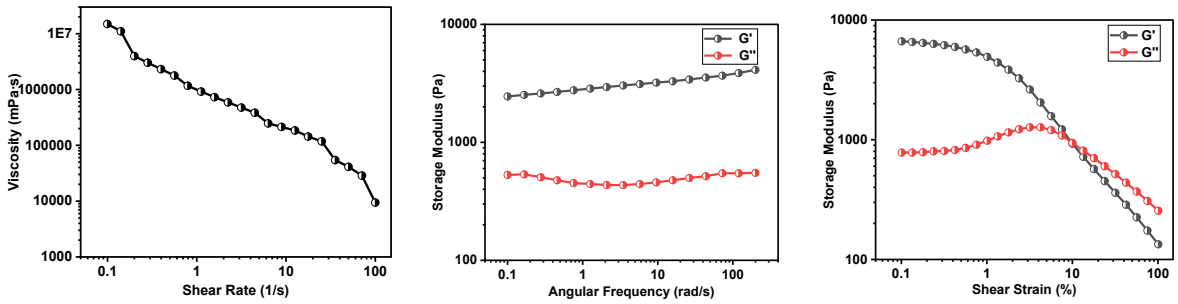

(a) (b) (c)

Figure 3(a-c): Rheological analysis of [Cho][Ala] based ionic hydrogel (a) viscosity measurement (b) Angular frequency test, (c) Stain sweep test.

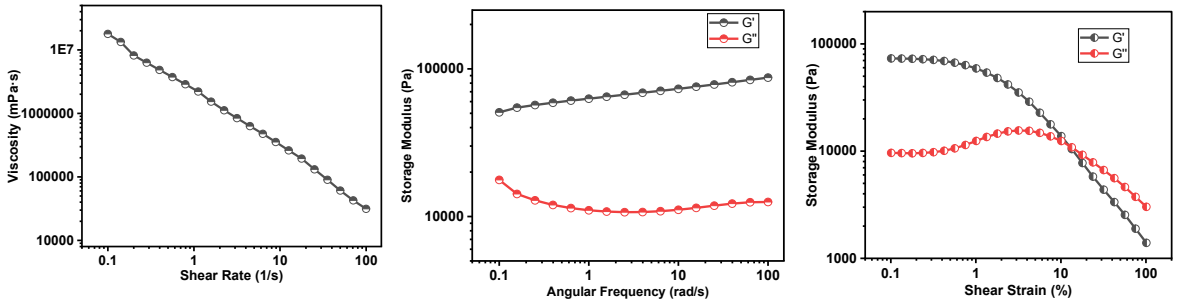

(d) (e) (f)

Figure 3(d-f): Rheological analysis of [Cho][Pro] based ionic hydrogel (d) viscosity measurement (e) Angular frequency test, (f) Stain sweep test.

For being the intelligent TDDDs, the hydrogel must undergo the self-healing behaviour. We used conventional visual observation test to investigate the self-healing behaviour for the studied ionic hydrogels where the circular shaped hydrogels with different colours were cut and placed in close contact with each other (**Figure 4a**). After 5 minutes, these both pieces of hydrogels seemed to self-healed and formation of whole one piece is seen. That was confirmed by stretching with the help of a pair of tongs and it was seen that the hydrogel did not break,

specially at the point where it was healed. These whole process shows that the hydrogel is having ability to self-heal without any external stimuli.

For more detailed elaboration, we have employed the relaxation test, in which the self-healing property being measured before and after applying external forces. As depicted in **Figure 4 b and c**, [Cho][Ala] and [Cho][Pro] based ionic hydrogels show the G' and G" at a lower strain value 5%, indicating the system is in the gel form. When the strain is increased to 30%, the value of G' decreased than that of G", which shows that the gel deformed. Again, reducing the strain to 5%, the value of G' increased than that of G", indicating the reformation of gel. This cycle was performed for the four times, and no significant changes were observed. These results suggest that hydrogels deform at higher strain value, and reverting back to their original form at lower strain value. This thixotropic behaviour suggests that the present ionic hydrogels are self-healable without external stimuli. This is due to breaking and reforming of non-covalent interactions between IL and OA.[39] Likewise, self-healing property of L-phenylalanine and β-amninoisobutyric acid based hydrogel was also explore by relaxation test, measured G' and G" at lower strain 0.1 % and higher strain 50% stain value.[40]

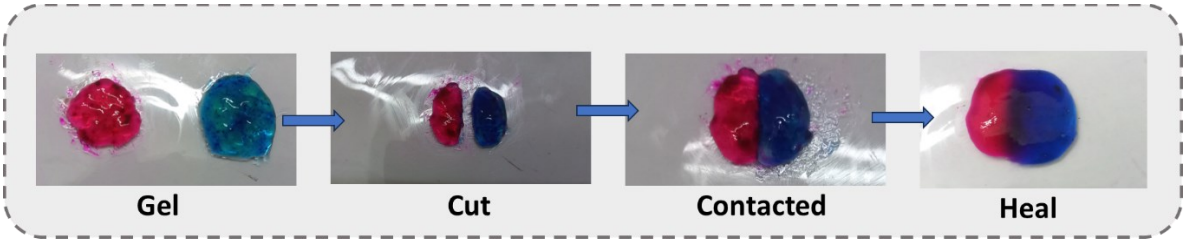

(a)

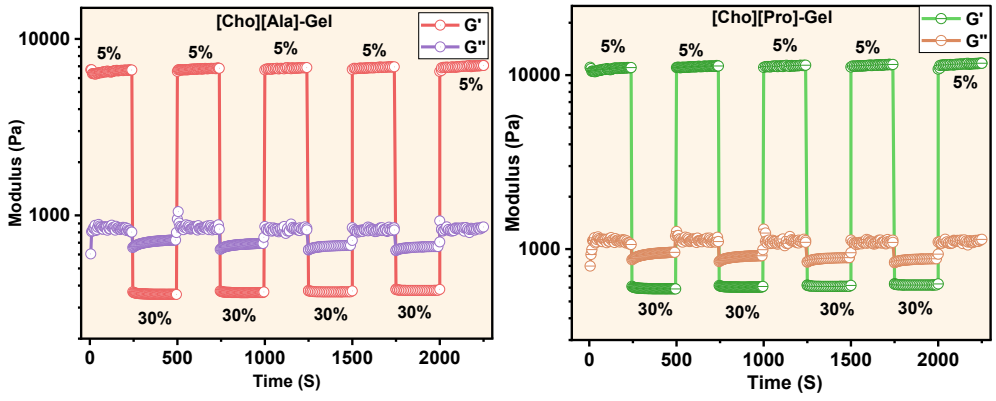

(b) (c)

Figure 4: (a) visual observation of self-healing, (b) relaxation test of [Cho][Ala] based system, (c) relaxation test of [Cho][Pro] based system.

Adhesive behaviour is crucial for the TDDSs, as the contact time with the skin significantly affects drug penetration.[41] As illustrated in **Figure 5a**, ionic hydrogel exhibits excellent adhesiveness to various materials such as skin, bone, muscles, steel, glass and plastic. Among them, skin, rubber and steel were used for a lap shear test, to measure the adhesive strength of ionic hydrogel (**Figure 5b**). The order of adhesive strength obtained for ionic hydrogel was: rubber (8.56kPa)> Skin (7.14 kPa) > steel (7.10kPa). The adhesive nature of ionic hydrogel is due to the presence of functional groups such as NH_2, OH, COO^-, and COOH, which are responsible for the non-covalent interactions with functional groups present on the surface of these materials (**Figure 5c**).[42] For the PAA/PE based hydrogel the adhesive strength with rubber was observed to be 4.2 kPa, for porcine skin 6.26 kPa and plastic was 7.3, suggesting that the studied ionic hydrogel have better adhesiveness than the polymeric hydrogel.[43]

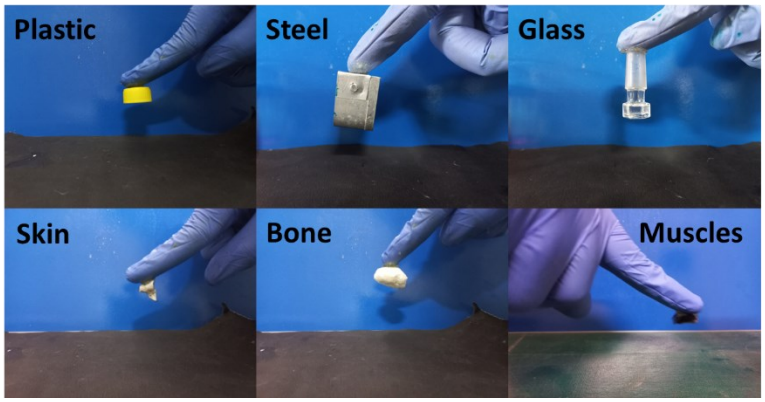

(a)

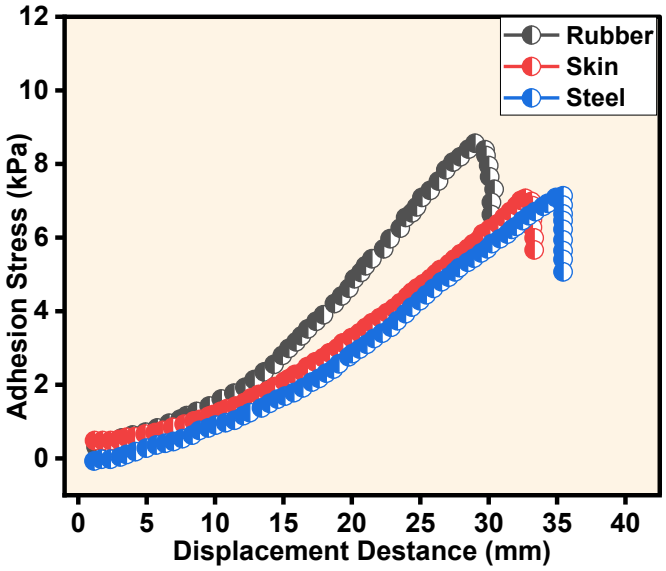

(b)

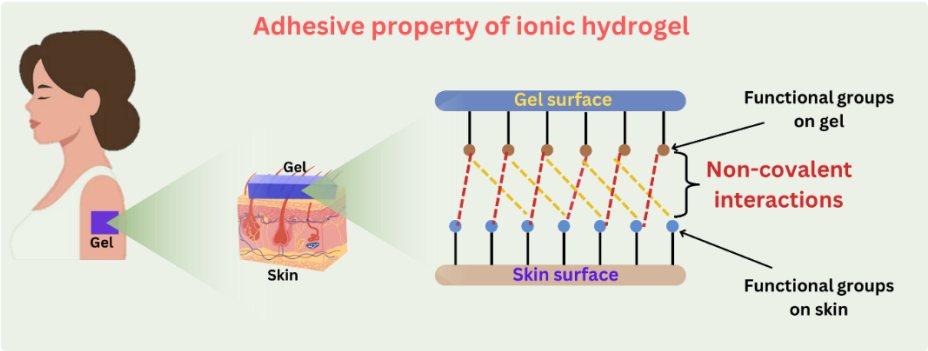

(c)

Figure 5: (a) Adhesiveness of ionic hydrogel with various materials, (b) Lap shear test of ionic hydrogel, (c) schematic representation of adhesive property.

It is of prime importance to investigate the thermal stability of the ionic hydrogel when it is to be used for the TDDS. As during the application, the hydrogel should not disintegrates because of temperature and pH of the skin, i.e. physiological conditions. We observed that the ionic hydrogel exhibited a reversible conversion of ionic hydrogel to a viscous flowing liquid as temperature increased from 25 °C to 110 °C ([IL]/[OA] = 0.84/0.66 M, **Figure S4 a**. The dramatic change is associated with the aggregates size or shape or both. When the

temperature of each ionic hydrogel was increased from 25 °C to 75 °C, the mesh size decreases (**Table S1**) and the intensity of peak in SANS curve also decreases (**Figure S4 b** and **c**). This is due to the weakening of the non-covalent interactions with temperature. Here, the hydrogel was converted into loose gel (**Figure S4 d**).[44,45] Muzammil and co-worker found similar observation for the amide functionalizied IL based hydrogel as the larger aggregates were converted into smaller aggreges at higher temperature.[29]

Furthermore, we applied DSC analysis to find the temperature (T_g) for gel to sol conversion. In the DSC graph, a distinct and sharp endothermic peak was arrived at 90 °C, and 110 °C for [Cho][Pro] and [Cho][Ala] based ionic hydrogel, respectively (**Figure S4 e**). These gel to sol conversion observed due to larger size aggregates that are converted in to small size aggregates at high temperature value.[29] Notably, T_g of [Cho][Ala] based ionic hydrogel is higher than that of [Cho][Pro] based ionic hydrogel. The reasons for above result are, unlike the alanine-based IL, the bulkiness of proline-based IL,[46] and the stronger interaction of OA with [Cho][Ala] compared to [Cho][Pro], leading to a lower temperature threshold for gel-to-sol conversion, FE-SEM results *vide infra*.[47] Remarkably, this conversion process exhibits complete reversibility; when the temperature decreases, the ionic hydrogel reverts back to its initial gel form. Comparable observation in gel to sol phase transition due to lamellar gel of [CetPy][Sal] converted into micelles solution at high temperature.[48]

Additionally, we have investigated the thermal stability of both ionic hydrogels, oleic acid as well as ILs through TGA analysis. A gradual degradation was observed in the TGA graph (**Figure S4 f)**. ILs and oleic acid are starting to degrade in the 150–160 °C and 200–220 °C temperature ranges, respectively. Furthermore, multi-step degradation observed in ionic hydrogels, in which the initial mass loss was observed at 100-110 °C, attributed to the evaporation of water.[49] Subsequently, a second mass loss occurred at 200-250 °C, attributed to the degradation of IL and OA.[50] For more visual and accurate understanding of gel to sol transition, the real time video is given **(Video S1)**.

We investigated the influence of pH on the sizes and shapes of aggregates in both ionic hydrogels. When the pH was reduced from 7.0 to 5.0 by adding 0.10 M HCl, both ionic hydrogels underwent a physical transformation into a sol state (**Figure 6a**). As the pH decreases, the conversion of gel like network to mixture of worm-like and ellipsoidal micelles was observed, due to the disruption of non-covalent interactions between IL and OA (**Figure 6b**).[51] This conversion is validated by SANS analysis (**Figure 6 c and d**). At acidic condition, pH-responsive functional groups such as NH_2, OH, COO^- and COOH become protonated, leading to the dissociation of intermolecular interaction between IL and OA. Additionally, due to protonation of these functional groups, reduction of interaction with water molecules can also observed.[52] The changes in aggregate shape and size are fundamentally due to this protonation process on functional groups of ionic hydrogels. Kalipada and a co-worker prepared amino acids-based pH-responsive systems that show phase separation at acidic pH system as at acidic pH, carboxylate group get protonated and that reduced their interaction with water.[53]

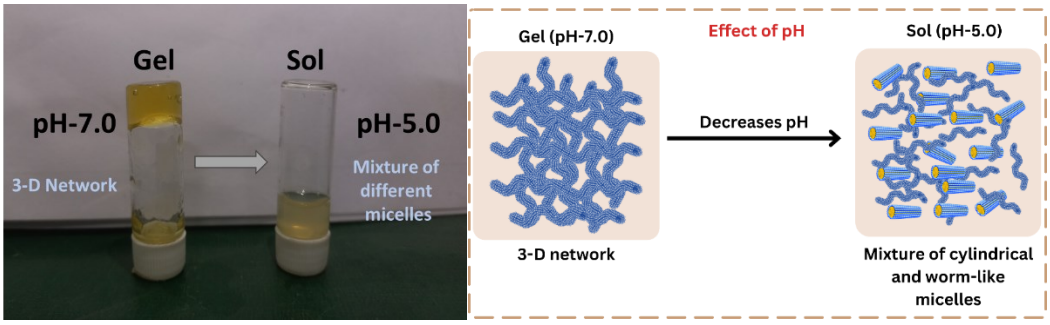

(a) (b)

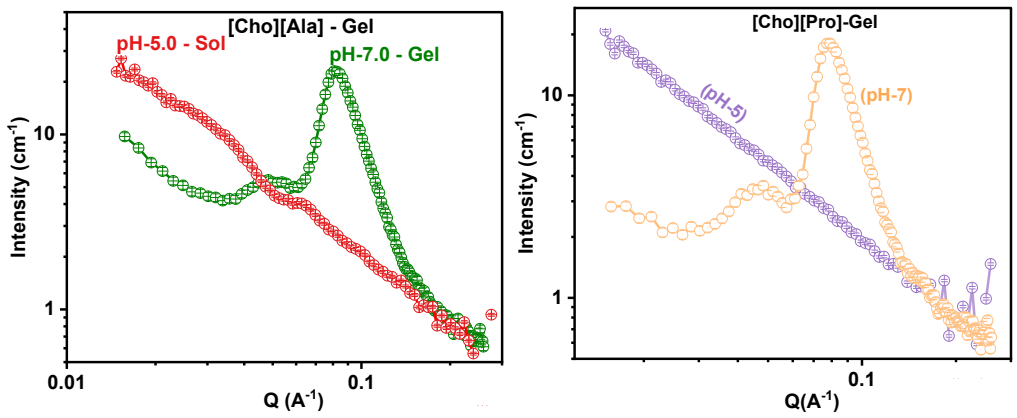

(c) (d)

Figure 6: (a) visual observation of effect of pH on ionic hydrogel, (b) schematic representation of pH effect, (c and d) SANS analysis of both ionic hydrogel at different pH value.

Drug loading in ionic hydrogel

The primary objective of this study is to develop a hydrogel with capability of encapsulating higher amount of anticancer drug. To achieve this, we started to dissolve 5-FU in an aqueous solution of ILs (0.84 M) to its saturation point, which is 156 mg/mL and 149 mg/mL for [Cho][Ala] and [Cho][Pro], respectively. After reaching the saturation point of 5-FU in ILs, OA was introduced for the formation of a drug loaded ionic hydrogels. This 3-D network of the ionic hydrogels contains the maximum possible amount of 5-FU drug. Subsequently, the drug concentration was determined using the UV spectroscopy. The encapsulated amount of 5-FU was 155 mg/mL and 147 mg/mL in [Cho][Ala] and [Cho][Pro] based ionic hydrogel, respectively, which is significantly higher than the water (12.2 mg/mL) and other organic solvents (5.5 mg/mL in 95 % ethanol, 8 mg/mL in pH-7.2 PBS and 53 mg/mL in DMSO). As shown in **Figure S5 a** and **d**, SANS analysis indicated that after drug loading, the mesh size of gel decreases, because 5-FU is interacted with gel through weak covalent bonding and entrapped within porous structure of hydrogel, and all SANS parameters for each systems are given in **Table S2**. Drug encapsulation capacity of [Cho][Ala] based hydrogel is higher as compare to [Cho][Pro] based hydrogel. As the molecular weight of alanine is quite lower as compare to proline, the presence of hydrotropic effect and more molecules at the same mass fraction, being the reason for the higher encapsulation.[19,54] In another way, smaller the molecule, more dissolving capacity and more electronegativity compared to large molecules.[55] Similar findings were reported for two drugs ibuprofen and acyclovir, where solubility of drug was observed higher in smaller anion compared to larger ones. The given reason for this finding is higher surface electron density of the alanine.[54]

In Vitro Biocompatibility of Ionic hydrogels

Biocompatibility plays a crucial role in terms of drug delivery systems, i.e., a drug delivery system with lower biocompatibility leads to effect some normal cells or tissues by itself.[56] We defended this statement by performing *in vitro* biocompatibility of both ionic hydrogels on normal cell lines (L-132 cells) as well as two different cancerous cell lines (MCF-7). As depicted in **Figure 7 (a and b)** and **Table S3**, for both ionic hydrogels at different concentration, cell viability of L-132 and MCF-7 cells was greater than 92% for 48 h. This is due to the biocompatible resources used in the formation of ionic hydrogels, such as amino acids and choline, which are essential nutrient for human body.[54,57] Additionally, OA is also used in formation of hydrogel, which is biocompatible too, and important energy source for normal human being.[58] As shown in **Table S3**, biocompatibility percentages shows that systems are possessing excellent biocompatibility and can be used as drug delivery systems. Similar results are observed for CAAILs on fibroblast cells line, where 92 % cell viability was observed after 48 h.[54] Amino acid and fatty acid based ILs were used for TDDSs by Goto and co-worker, where authors noted that 93 % of normal cells were viable after 48 h.[19]

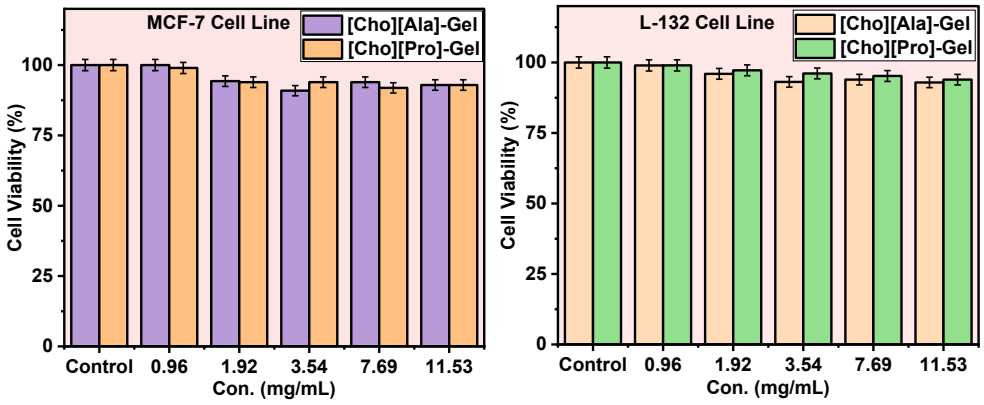

(a) (b)

Figure 7: *In vitro* biocompatibility of both ionic hydrogel on (a) cancerous cell line MCF-7, (b) normal cell line L-132.

In vitro permeation study of 5-FU

It is necessary to surmount the SC barrier in order to permeate drug molecules through skin effectively.[59] The essential requirements for permeation of drug

through skin are; a drug molecular weight should be less than 500 Da, it must have significant lipophilicity (log octanol-water partition coefficient between 1-3) and melting must be less than 200 °C.[60] As 5-FU is having a log octanol-water coefficient of -0.89, which makes it difficult in penetration.[61] We overcome this difficulty by encapsulating 5-FU within ionic hydrogels. We investigated the *in vitro* skin permeation of 5-FU using goat skin through the Franz diffusion cell at 32 °C and 48 h (**Figure 8a**). The reason for using the goat skin is the similarity between biological characteristics with human skin.[62] Here, we investigated the permeation of 5-FU in ionic hydrogels, and PBS used as control system (**Figure 8b**). As shown in **Table 3**, the permeated amount of 5-FU is 255 µM, 250 µM, and 0.001 µM for [Cho][Ala], [Cho][Pro] based ionic hydrogel and PBS, respectively (**Figure 8c**). Without OA, the permeated amount of 5-FU are 9 µM and 8 µM in [Cho][Ala] and [Cho][Pro], respectively. Other transdermal permeation parameters for ionic hydrogels are given in **Table 3**. As penetration enhancer OA is present in both systems, both systems show almost same permeation of 5-FU in the skin. Generally, most of fatty acids possesses good enhancement capacity for skin penetration.[63] Among them, OA contains one unsaturation in form of π-bond, has the capability to establish π-π interactions with the stratum coronium (SC) layer, which can enhance the skin permeation of drug molecules.[64,65] These interactions were observed in both ionic hydrogels, resulting in superior skin permeation, compared to traditional skin permeation enhancers such as Tween-80 and other CPE.[19] These findings suggest that [Cho][Ala] and [Cho][Pro]-based ionic hydrogels possess the potential for effective transdermal drug delivery.

Table 3: The skin permeation parameters of both ionic hydrogels.

Formulations	**Transdermal Flux J (ug/cm²/h)**	**t_L (h)**	**Kp(cm/h)**
[Cho][Ala]-Gel	13.12	48.00	1.3
[Cho][Pro]-Gel	12.52	48.00	1.2

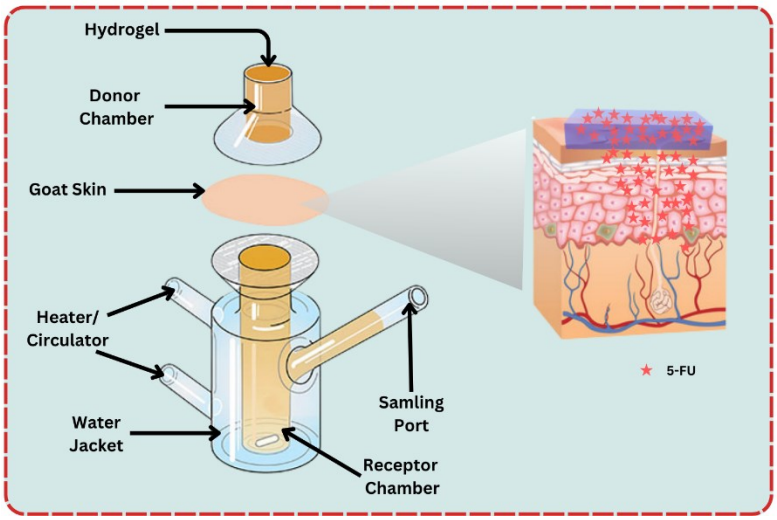

(a)

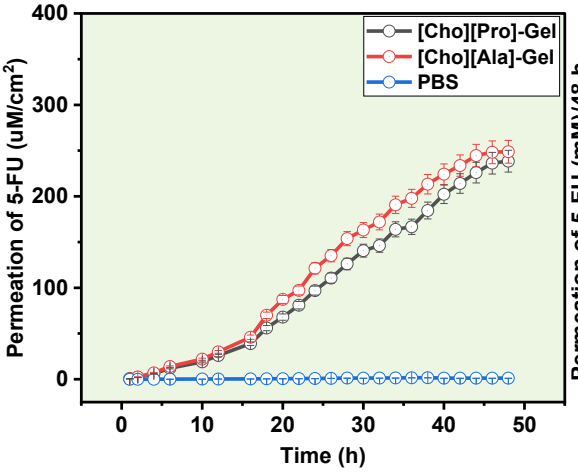

(b)

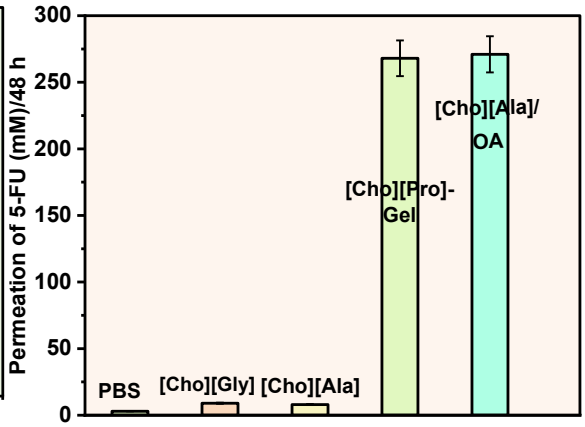

(c)

Figure 8: (a) Schematic representation of Frazan diffusion cell (b) permeation profile of 5-FU from ionic hydrogels (c) permeation amount of 5-FU in PBS, ILs and Ionic hydrogels.

Skin penetration mechanism

A Franz diffusion cell technique was used to investigate the effect in the present ionic hydrogels on the structure of the stratum corneum (SC). Following that, FTIR analysis were performed to determine changes in the intracellular lipid content inside the SC. In general, lipid fluidization and/or lipid extraction from SC layer are responsible mechanisms for enhancement of skin permeability of drug molecules.[9,66] The shift in the CH_2 symmetric and CH_2 asymmetric stretching

vibrations, 2850 cm^{-1} and 2920 cm^{-1} respectively, and/or the decrease in the lipid peak area at approximately 2850 cm^{-1} suggests that lipid fluidization and lipid extraction was observed in SC layer.[14,67] The peaks attributed to keratin and lipid of SC layer is shown in **Figure S6**. In PBS (control), the typical peaks for lipid chains and keratin are represented by 1738 cm^{-1}(C=O vibration), 2851.65 (CH_2 symmetric stretching vibration), 2920.12 cm^{-1} (CH_2 asymmetric stretching vibration), and 1638.80 cm^{-1}, 1539.32 cm^{-1} for NH-C=O. Notably, both these typical peaks for SC lipid and keratin showed substantial positive shifts in both ionic hydrogels (**Table S4)**. In comparison, the [Cho][Ala] based system shows a stronger impact regarding the penetration, than the [Cho][Pro] based system. The CH_2 symmetric and asymmetric vibrations in the [Cho][Ala] based system, shifted to 2928.23 cm^{-1} and 2857.63 cm^{-1}, respectively. Also in keratin, the C=O vibration frequency (1745 cm^{-1}) and NH-C=O vibrations was changed to 1643.23 cm^{-1} and 1545.42 cm^{-1}. Peak shifted due to [Cho][Pro] based system was given in **Table S4**. These changes corresponded with the SC lipid layer, the changes are shown from a predominantly lamellar Cr-state to a more fluid state, suggests that the lipid fluidization brought by IL and OA.[19,66] These finding are essential for facilitating the penetration of drug molecules into the skin. The ionic hydrogels are presumed to permeate the SC lipid bilayers and partition within them, weakening interlipid interactions due to the hydrophobic nature of OA and ionic nature of [Cho][Ala] and [Cho][Prol]. Furthermore, the OA present in ionic hydrogel is capable of increasing SC hydration, further contributing to lipid bilayer fluidization.[14] Additionally, the hydrophobic properties of ionic hydrogel led to shift in characteristic peak in SC bilayers (**Figure S6 and Table S4**).

In vitro histological analysis

In vitro histological analysis was performed to evaluate the biocompatibility and safety profiles of the investigated ionic hydrogels. As shown in the microscopy image of skin treated with PBS as a control, no significant change was observed on the epidermis, dermis, or subcutaneous tissue of the skin layers (**Figure 9a**). When ionic hydrogel is treated with skin, the layer of skin is clearly visible and organised, and no significant damage was observed, as shown in **Figure 9 b** and

c. This result indicated that both hydrogels do not show harmful effects on skin when used as TDDSs.

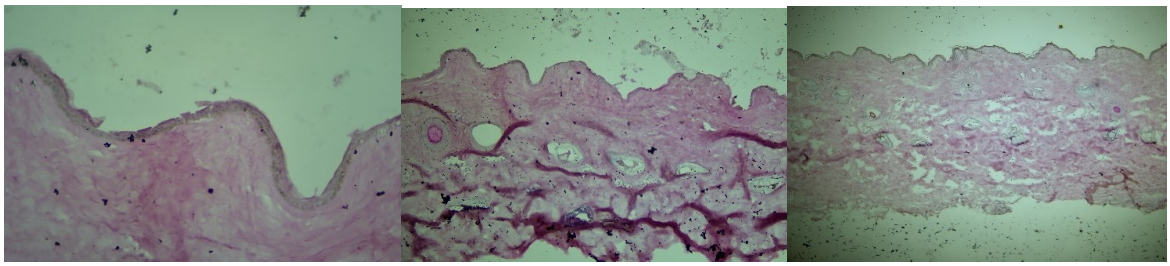

(a) (b) (c)

Figure 9: Microscopic image of histological analysis of the skin treated with (a) PBS (Control), (b) [Cho][Ala]/OA based ionic hydrogel, (c) [Cho][Pro]/OA based ionic hydrogel.

In Vitro Cytotoxicity

The 5-FU-free ionic hydrogels exhibited excellent biocompatibility with negligible cytotoxicity observed on normal cells as well as cancerous cells, as mentioned earlier. To determine the effectiveness and required doses of 5-FU-loaded ionic hydrogels for tumour cell inhibition, *in vitro* cytotoxicity study was employed.[61] For this purpose, we used cancerous cell lines such as MCF-7 and HeLa.[68] The obtained IC_{50} values for MCF-7 and HeLa cell lines are 2.15 mM and 0.75 mM for [Cho][Ala]-based ionic hydrogel after 48 h, respectively (**Figure 10 a, b**). Similarly, we obtained 2.65 mM and 1.50 mM IC_{50} values for [Cho][Pro]-based ionic hydrogel after 48 h, respectively. These findings suggest that systems possess good cytotoxicity with lower doses, on cancerous cell lines.

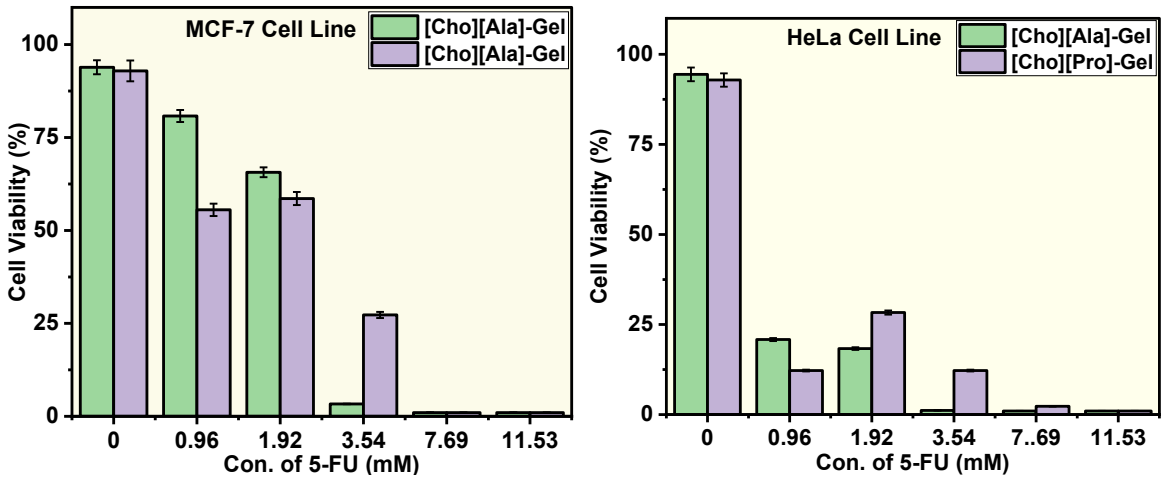

(a) (b)

Figure 10: *In vitro* cytotoxicity of 5-FU loaded ionic hydrogels on (a) MCF-7 cell line and (b) HeLa cell line.

Conclusion

In this research, we have prepared successfully two different ionic hydrogels through synergistically interacting [Cho][Ala] and [Cho][Pro] with OA and analysed them using SANS, FTIR, FE-SEM, EDX, DSC and TGA techniques. The mechanism of formation, morphology, mechanical properties, physical and thermal stability of the ionic hydrogels are also investigated. The hydrogels exhibited excellent *in vitro* biocompatibility. As results shows, when cells were treated with different concentrations of hydrogel, the viability of normal and cancerous cells was above 92% after 48 h. The ionic hydrogels were found to enhance the permeability of the hydrophilic drug 5-FU through the skin by making the intracellular lipid of the SC layer more fluid. Interestingly, the both ionic hydrogels showed significantly greater permeation of 5-FU compare to PBS and other conventional chemical enhancer. Among both, [Cho][Ala] based ionic hydrogel show greater skin permeability compared to [Cho][Pro] based ionic hydrogel. That can potentially overcome the challenges of delivering hydrophilic drug through the skin. *In vitro* cytotoxicity results revealed the synergistic anticancer impact of 5-FU-loaded ionic hydrogels on MCF-7 and HeLa cell lines with lower dosage values. These findings suggest that newly introduced ionic

hydrogels hold a promising approach for the treatment of breast cancer in a transdermal way. Nevertheless, further research still requires *in vivo* clinical behaviour study before considering the use of ionic hydrogels in breast cancer treatment.

Supporting Information

^{1}H-NMR spectra of [Cho][Ala] and [Cho][Pro], FTIR and EDX spectra of both ionic hydrogels, effect of temperature on system including SANS, TGA, DSC, visual observation as well as graphical interaction and SANS scatting plot of drug loaded systems and FTIR spectra of the SC layer after treatment with hydrogels are provided in ESI file.

Acknowledgments

NM acknowledges the financial assistance of UGC-DAE for the Collaborative Research Scheme (UDCSR/MUM/AO/CRS-M-997/2023).

Author contributions

Ravi Pansuriya	**:** Conceptualization, methodology, writing-original draft and visualization.
Tapas Patel	**:** Conceptualization, methodology, writing-original draft and visualization.
Sugam Kumar	**:** Conceptualization, methodology,
Vinod K Aswal	**:** Conceptualization, methodology,
Naina Raje	**:** Conceptualization, methodology,
Clare Hoskins	**:** Writing-original draft and visualization.
Sursh Kumar Kailasa	**:** Conceptualization, methodology,
Naved I. Malek	**:** Conceptualization, Supervision, writing-review and editing, funding acquisition.

All authors have given approval to the final version of the manuscript.

Conflicts of interest

There are no conflicts to declare.

Reference

(1) Chen, S.; Liu, Y.; Fong, D. Y. T.; Zhou, J.; Chen, H.; Wan, C. Health-Related Quality of Life and Its Influencing Factors in Patients with Breast Cancer Based on the Scale QLICP-BR. *Sci. Rep.* **2023**, *13* (1), 15176.

(2) Bray, F.; Ferlay, J.; Soerjomataram, I.; Siegel, R. L.; Torre, L. A.; Jemal, A. Global Cancer Statistics 2018: GLOBOCAN Estimates of Incidence and Mortality Worldwide for 36 Cancers in 185 Countries. *CA. Cancer J. Clin.* **2018**, *68* (6), 394–424.

(3) Chakraborty, S.; Rahman, T. The Difficulties in Cancer Treatment. *Ecancermedicalscience* **2012**, *6*, ed16.

(4) Prausnitz, M. R.; Langer, R. Transdermal Drug Delivery. *Nat. Biotechnol.* **2008**, *26* (11), 1261–1268.

(5) Alkilani, A.; McCrudden, M. T.; Donnelly, R. Transdermal Drug Delivery: Innovative Pharmaceutical Developments Based on Disruption of the Barrier Properties of the Stratum Corneum. *Pharmaceutics* **2015**, *7* (4), 438–470.

(6) Paudel, K. S.; Milewski, M.; Swadley, C. L.; Brogden, N. K.; Ghosh, P.; Stinchcomb, A. L. Challenges and Opportunities in Dermal/Transdermal Delivery. *Ther. Deliv.* **2010**, *1* (1), 109–131..

(7) Ramadon, D.; McCrudden, M. T. C.; Courtenay, A. J.; Donnelly, R. F. Enhancement Strategies for Transdermal Drug Delivery Systems: Current Trends and Applications. *Drug Deliv. Transl. Res.* **2022**, *12* (4), 758–791.

(8) Moghadam, S. H.; Saliaj, E.; Wettig, S. D.; Dong, C.; Ivanova, M. V.; Huzil, J. T.; Foldvari, M. Effect of Chemical Permeation Enhancers on Stratum Corneum Barrier Lipid Organizational Structure and Interferon Alpha Permeability. *Mol. Pharm.* **2013**, *10* (6), 2248–2260.

(9) Banerjee, A.; Ibsen, K.; Iwao, Y.; Zakrewsky, M.; Mitragotri, S. Transdermal

Protein Delivery Using Choline and Geranate (CAGE) Deep Eutectic Solvent. *Adv. Healthc. Mater.* **2017**, *6* (15), 1601411.

(10) Pathan, I.; Setty, C. Chemical Penetration Enhancers for Transdermal Drug Delivery Systems. *Trop. J. Pharm. Res.* **2009**, *8* (2), 173-179.

(11) Ibrahim, S. A.; Li, S. K. Efficiency of Fatty Acids as Chemical Penetration Enhancers: Mechanisms and Structure Enhancement Relationship. *Pharm. Res.* **2010**, *27* (1), 115–125.

(12) Kováčik, A.; Kopečná, M.; Hrdinová, I.; Opálka, L.; Boncheva Bettex, M.; Vávrová, K. Time-Dependent Differences in the Effects of Oleic Acid and Oleyl Alcohol on the Human Skin Barrier. *Mol. Pharm.* **2023**, *20* (12), 6237–6245.

(13) Lei, Z.; Chen, B.; Koo, Y.-M.; MacFarlane, D. R. Introduction: Ionic Liquids. *Chem. Rev.* **2017**, *117* (10), 6633–6635.

(14) Md Moshikur, R.; Shimul, I. M.; Uddin, S.; Wakabayashi, R.; Moniruzzaman, M.; Goto, M. Transformation of Hydrophilic Drug into Oil-Miscible Ionic Liquids for Transdermal Drug Delivery. *ACS Appl. Mater. Interfaces* **2022**, *14* (50), 55332–55341.

(15) Klebeko, J.; Krüger, O.; Dubicki, M.; Ossowicz-Rupniewska, P.; Janus, E. Isopropyl Amino Acid Esters Ionic Liquids as Vehicles for Non-Steroidal Anti-Inflammatory Drugs in Potential Topical Drug Delivery Systems with Antimicrobial Activity. *Int. J. Mol. Sci.* **2022**, *23* (22), 13863.

(16) Tanner, E. E. L.; Curreri, A. M.; Balkaran, J. P. R.; Selig-Wober, N. C.; Yang, A. B.; Kendig, C.; Fluhr, M. P.; Kim, N.; Mitragotri, S. Design Principles of Ionic Liquids for Transdermal Drug Delivery. *Adv. Mater.* **2019**, *31* (27). e1901103.

(17) Pedro, S. N.; R. Freire, C. S.; Silvestre, A. J. D.; Freire, M. G. The Role of Ionic Liquids in the Pharmaceutical Field: An Overview of Relevant Applications. *Int. J. Mol. Sci.* **2020**, *21* (21), 8298.

(18) Wilms, W.; Woźniak-Karczewska, M.; Syguda, A.; Niemczak, M.; Ławniczak,

Ł.; Pernak, J.; Rogers, R. D.; Chrzanowski, Ł. Herbicidal Ionic Liquids: A Promising Future for Old Herbicides? Review on Synthesis, Toxicity, Biodegradation, and Efficacy Studies. *J. Agric. Food Chem.* **2020**, *68* (39), 10456–10488.

(19) Md Moshikur, R.; Chowdhury, M. R.; Fujisawa, H.; Wakabayashi, R.; Moniruzzaman, M.; Goto, M. Design and Characterization of Fatty Acid-Based Amino Acid Ester as a New "Green" Hydrophobic Ionic Liquid for Drug Delivery. *ACS Sustain. Chem. Eng.* **2020**, *8* (36), 13660–13671.

(20) Mitchell, M. J.; Billingsley, M. M.; Haley, R. M.; Wechsler, M. E.; Peppas, N. A.; Langer, R. Engineering Precision Nanoparticles for Drug Delivery. *Nat. Rev. Drug Discov.* **2021**, *20* (2), 101–124.

(21) Pitakjakpipop, H.; Rajan, R.; Tantisantisom, K.; Opaprakasit, P.; Nguyen, D. D.; Ho, V. A.; Matsumura, K.; Khanchaitit, P. Facile Photolithographic Fabrication of Zwitterionic Polymer Microneedles with Protein Aggregation Inhibition for Transdermal Drug Delivery. *Biomacromolecules* **2022**, *23* (1), 365–376.

(22) Buwalda, S. J.; Vermonden, T.; Hennink, W. E. Hydrogels for Therapeutic Delivery: Current Developments and Future Directions. *Biomacromolecules* **2017**, *18* (2), 316–330.

(23) Li, J.; Mooney, D. J. Designing Hydrogels for Controlled Drug Delivery. *Nat. Rev. Mater.* **2016**, *1* (12), 16071.

(24) Gao, Y.; Hao, Y.; Zhang, W.; Wei, Y.; Shu, Y.; Wang, J. Microwave-Triggered Ionic Liquid-Based Hydrogel Dressing with Excellent Hyperthermia and Transdermal Drug Delivery Performance. *Chem. Eng. J.* **2022**, *429*, 131590.

(25) Miao, S.; Atkin, R.; Warr, G. Design and Applications of Biocompatible Choline Amino Acid Ionic Liquids. *Green Chem.* **2022**, *24* (19), 7281–7304.

(26) Suga, K.; Kondo, D.; Otsuka, Y.; Okamoto, Y.; Umakoshi, H. Characterization of Aqueous Oleic Acid/Oleate Dispersions by Fluorescent Probes and Raman Spectroscopy. *Langmuir* **2016**, *32* (30), 7606–7612.

(27) Pavez, P.; Figueroa, R.; Medina, M.; Millán, D.; Falcone, R. D.; Tapia, R. A. Choline [Amino Acid] Ionic Liquid/Water Mixtures: A Triple Effect for the Degradation of an Organophosphorus Pesticide. *ACS Omega* **2020**, *5* (41), 26562–26572.

(28) Curtis, J. E.; McAuley, A.; Nanda, H.; Krueger, S. Protein Structure and Interactions in the Solid State Studied by Small-Angle Neutron Scattering. *Faraday Discuss.* **2012**, *158*, 285.

(29) Kuddushi, M.; Kumar, A.; Ray, D.; Aswal, V. K.; El Seoud, O. A.; Malek, N. I. Concentration- and Temperature-Responsive Reversible Transition in Amide-Functionalized Surface-Active Ionic Liquids: Micelles to Vesicles to Organogel. *ACS Omega* **2020**, *5* (38), 24272–24284.

(30) Gontsarik, M.; Mohammadtaheri, M.; Yaghmur, A.; Salentinig, S. PH-Triggered Nanostructural Transformations in Antimicrobial Peptide/Oleic Acid Self-Assemblies. *Biomater. Sci.* **2018**, *6* (4), 803–812.

(31) Yang, K.; Peng, H.; Wen, Y.; Li, N. Re-Examination of Characteristic FTIR Spectrum of Secondary Layer in Bilayer Oleic Acid-Coated Fe3O4 Nanoparticles. *Appl. Surf. Sci.* **2010**, *256* (10), 3093–3097.

(32) Prentø, P. The Role of Glycine and Prolines in Connective Tissue Fiber Staining with Hydrogen Bonding Dyes. *Biotech. Histochem.* **2007**, *82* (4–5), 199–200.

(33) Gayen, K.; Basu, K.; Bairagi, D.; Castelletto, V.; Hamley, I. W.; Banerjee, A. Amino-Acid-Based Metallo-Hydrogel That Acts Like an Esterase. *ACS Appl. Bio Mater.* **2018**, *1* (5), 1717–1724.

(34) Kuddushi, M.; Patel, N. K.; Rajput, S.; El Seoud, O. A.; Mata, J. P.; Malek, N. I. Temperature-Responsive Low Molecular Weight Ionic Liquid Based Gelator: An Approach to Fabricate an Anti-Cancer Drug-Loaded Hybrid Ionogel. *ChemSystemsChem* **2020**, *2* (5), e1900053.

(35) Scimeca, M.; Bischetti, S.; Lamsira, H. K.; Bonfiglio, R.; Bonanno, E. Energy Dispersive X-Ray (EDX) Microanalysis: A Powerful Tool in Biomedical

Research and Diagnosis. *Eur. J. Histochem.* **2018**, *62*(2), 2841.

(36) Eivazzadeh-Keihan, R.; Pajoum, Z.; Aliabadi, H. A. M.; Mohammadi, A.; Kashtiaray, A.; Bani, M. S.; Pishva, B.; Maleki, A.; Heravi, M. M.; Mahdavi, M.; Ziaei Ziabari, E. Magnetized Chitosan Hydrogel and Silk Fibroin, Reinforced with PVA: A Novel Nanobiocomposite for Biomedical and Hyperthermia Applications. *RSC Adv.* **2023**, *13* (13), 8540–8550.

(37) Stojkov, G.; Niyazov, Z.; Picchioni, F.; Bose, R. K. Relationship between Structure and Rheology of Hydrogels for Various Applications. *Gels* **2021**, *7* (4), 255.

(38) Arokianathan, J. F.; Ramya, K. A.; Janeena, A.; Deshpande, A. P.; Ayyadurai, N.; Leemarose, A.; Shanmugam, G. Non-Proteinogenic Amino Acid Based Supramolecular Hydrogel Material for Enhanced Cell Proliferation. *Colloids Surfaces B Biointerfaces* **2020**, *185*, 110581.

(39) Kuddushi, M.; Deng, X.; Nayak, J.; Zhu, S.; Xu, B. Bin; Zhang, X. A Transparent, Tough and Self-Healable Biopolymeric Composites Hydrogel for Open Wound Management. *ACS Appl. Bio Mater.* **2023**, *6* (9), 3810–3822.

(40) Nandi, S. K.; Maji, K.; Haldar, D. Self-Healing Hydrogel from a Dipeptide and HCl Sensing. *ACS Omega* **2018**, *3* (4), 3744–3751.

(41) Kim, Y. E.; Jung, H. Y.; Park, N.; Kim, J. Adhesive Composite Hydrogel Patch for Sustained Transdermal Drug Delivery To Treat Atopic Dermatitis. *Chem. Mater.* **2023**, *35* (3), 1209–1217.

(42) Jung, H.; Kim, M. K.; Lee, J. Y.; Choi, S. W.; Kim, J. Adhesive Hydrogel Patch with Enhanced Strength and Adhesiveness to Skin for Transdermal Drug Delivery. *Adv. Funct. Mater.* **2020**, *30* (42), 2004407.

(43) Li, W.; Feng, R.; Wang, R.; Li, D.; Jiang, W.; Liu, H.; Guo, Z.; Serpe, M. J.; Hu, L. Polyelectrolyte-Based Physical Adhesive Hydrogels with Excellent Mechanical Properties for Biomedical Applications. *J. Mater. Chem. B* **2018**, *6* (29), 4799–4807.

(44) Qin, J.; Sun, M.; Hu, W.; Cheng, J.; Fan, Z.; Du, J. Stimuli-Responsive

Hydrogels for Cancer Immunotherapy. *Polym. Chem.* **2023**, *14* (7), 793–802.

(45) Pansuriya, R.; Patel, T.; Mehra, S.; Kumar, A.; El Seoud, O. A.; Kumar, S.; Aswal, V. K.; Kailasa, S. K.; Malek, N. I. A Dual Responsive Ionic Liquid-Based Polymeric Hydrogel: A Promising Drug Delivery Vehicle for the Treatment of Breast Cancer. *New J. Chem.* **2023**, *47* (30), 14261–14272.

(46) Krieger, F.; Möglich, A.; Kiefhaber, T. Effect of Proline and Glycine Residues on Dynamics and Barriers of Loop Formation in Polypeptide Chains. *J. Am. Chem. Soc.* **2005**, *127* (10), 3346–3352.

(47) Körner, P. Hydrothermal Degradation of Amino Acids. *ChemSusChem* **2021**, *14* (22), 4947–4957.

(48) Kuddushi, M.; Patel, N. K.; Rajput, S.; El Seoud, O. A.; Mata, J. P.; Malek, N. I. Temperature-Responsive Low Molecular Weight Ionic Liquid Based Gelator: An Approach to Fabricate an Anti-Cancer Drug-Loaded Hybrid Ionogel. *ChemSystemsChem* **2020**, *2* (5), e1900053.

(49) Lai, W.-F.; Reddy, O. S.; Law, L.; Wu, H.; Wong, W.-T. A Self-Indicating and Antibacterial Gelatine–Chitosan Blended Hydrogel Enabling Real-Time Quality Control and Sustained Bioactive Agent Delivery. *RSC Adv.* **2023**, *13* (17), 11865–11873.

(50) Lease, J.; Kawano, T.; Andou, Y. Effect of Cellulose Materials on the Mechanochemical-Assisted Reaction System with Oleic Acid. *RSC Adv.* **2023**, *13* (39), 27558–27567.

(51) Edirisinghe, D. I. U.; D'Souza, A.; Ramezani, M.; Carroll, R. J.; Chicón, Q.; Muenzel, C. L.; Soule, J.; Monroe, M. B. B.; Patteson, A. E.; Makhlynets, O. V. Antibacterial and Cytocompatible PH-Responsive Peptide Hydrogel. *Molecules* **2023**, *28* (11), 4390.

(52) Rufino, A. F. C. S.; Bola, J. M.; Capela, E. V.; Coutinho, J. A. P.; e Silva, F. A.; Freire, M. G. Double-Stimuli-Responsive (Temperature and PH) Aqueous Biphasic Systems Comprising Ionic Liquids. *ACS Sustain. Chem. Eng.* **2023**, *11* (16), 6343–6351.

(53) Manna, K.; Patra, P.; Roy, A.; Roy, R. K.; Chaitanya Sunka, K.; Dhara, S.; Patra, N.; Pal, S. Amino Acid Inspired Alginate-Based PH Sensitive Polymeric Micelles via Reversible Addition–Fragmentation Chain Transfer Polymerization. *ACS Appl. Polym. Mater.* **2022**, *4* (6), 4432–4444.

(54) Islam, M. R.; Chowdhury, M. R.; Wakabayashi, R.; Tahara, Y.; Kamiya, N.; Moniruzzaman, M.; Goto, M. Choline and Amino Acid Based Biocompatible Ionic Liquid Mediated Transdermal Delivery of the Sparingly Soluble Drug Acyclovir. *Int. J. Pharm.* **2020**, *582*, 119335.

(55) Yuan, J.; Wu, J.; Yin, T. Solubility and Permeation Enhancement of Poor Soluble Drug by Cholinium-Amino Acid Based Ionic Liquids. *J. Drug Deliv. Sci. Technol.* **2020**, *60*, 102037.

(56) Han, G.-M.; Liu, B.; Kong, D. M.; Zhu, L.-N. DNA as Highly Biocompatible Carriers for Drug Delivery. *Mater. Chem. Front.* **2023**, *7*, 6345-6365.

(57) Zeisel, S. H.; da Costa, K. A. Choline: An Essential Nutrient for Public Health. *Nutr. Rev.* **2009**, *67* (11), 615–623.

(58) Liu, X.; Ma, D.; Tang, H.; Tan, L.; Xie, Q.; Zhang, Y.; Ma, M.; Yao, S. Polyamidoamine Dendrimer and Oleic Acid-Functionalized Graphene as Biocompatible and Efficient Gene Delivery Vectors. *ACS Appl. Mater. Interfaces* **2014**, *6* (11), 8173–8183.

(59) Neupane, R.; Boddu, S. H. S.; Abou-Dahech, M. S.; Bachu, R. D.; Terrero, D.; Babu, R. J.; Tiwari, A. K. Transdermal Delivery of Chemotherapeutics: Strategies, Requirements, and Opportunities. *Pharmaceutics* **2021**, *13* (7), 960.

(60) Jiang, T.; Wang, T.; Li, T.; Ma, Y.; Shen, S.; He, B.; Mo, R. Enhanced Transdermal Drug Delivery by Transfersome-Embedded Oligopeptide Hydrogel for Topical Chemotherapy of Melanoma. *ACS Nano* **2018**, *12* (10), 9693–9701.

(61) Safwat, M. A.; Soliman, G. M.; Sayed, D.; Attia, M. A. Fluorouracil-Loaded Gold Nanoparticles for the Treatment of Skin Cancer: Development, in Vitro

Characterization, and in Vivo Evaluation in a Mouse Skin Cancer Xenograft Model. *Mol. Pharm.* **2018**, *15* (6), 2194–2205.

(62) Neupane, R.; Boddu, S. H. S.; Renukuntla, J.; Babu, R. J.; Tiwari, A. K. Alternatives to Biological Skin in Permeation Studies: Current Trends and Possibilities. *Pharmaceutics* **2020**, *12* (2), 152.

(63) Islam, M. R.; Chowdhury, M. R.; Wakabayashi, R.; Kamiya, N.; Moniruzzaman, M.; Goto, M. Ionic Liquid-In-Oil Microemulsions Prepared with Biocompatible Choline Carboxylic Acids for Improving the Transdermal Delivery of a Sparingly Soluble Drug. *Pharmaceutics* **2020**, *12* (4), 392.

(64) Funakoshi, Y.; Iwao, Y.; Noguchi, S.; Itai, S. Effect of Alkyl Chain Length and Unsaturation of the Phospholipid on the Physicochemical Properties of Lipid Nanoparticles. *Chem. Pharm. Bull. (Tokyo).* **2015**, *63* (9), 731–736.

(65) Schwarz, J. C.; Pagitsch, E.; Valenta, C. Comparison of ATR–FTIR Spectra of Porcine Vaginal and Buccal Mucosa with Ear Skin and Penetration Analysis of Drug and Vehicle Components into Pig Ear. *Eur. J. Pharm. Sci.* **2013**, *50* (5), 595–600.

(66) Moshikur, R. M.; Chowdhury, M. R.; Wakabayashi, R.; Tahara, Y.; Kamiya, N.; Moniruzzaman, M.; Goto, M. Ionic Liquids with N-Methyl-2-Pyrrolidonium Cation as an Enhancer for Topical Drug Delivery: Synthesis, Characterization, and Skin-Penetration Evaluation. *J. Mol. Liq.* **2020**, *299*, 112166.

(67) Lu, B.; Liu, T.; Wang, H.; Wu, C.; Chen, H.; Liu, Z.; Zhang, J. Ionic Liquid Transdermal Delivery System: Progress, Prospects, and Challenges. *J. Mol. Liq.* **2022**, *351*, 118643.

(68) Farasati Far, B.; Omrani, M.; Naimi Jamal, M. R.; Javanshir, S. Multi-Responsive Chitosan-Based Hydrogels for Controlled Release of Vincristine. *Commun. Chem.* **2023**, *6* (1), 28.

Table of Content